

Closing the Cyan Gap Toward Full-Spectrum LED Lighting with NaMgBO₃:Ce³⁺

Jiyou Zhong,^{||} Ya Zhuo,^{||} Shruti Hariyani, Weiren Zhao,* Jun Wen, and Jakoah Brgoch*



Cite This: *Chem. Mater.* 2020, 32, 882–888



Read Online

ACCESS |



Metrics & More

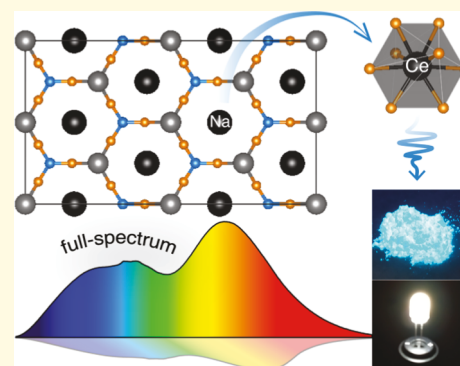


Article Recommendations



Supporting Information

ABSTRACT: The photoluminescence spectrum generated by an ordinary phosphor-converted white light-emitting diode (pc-wLED) that combines a blue LED chip with a yellow phosphor or a near-UV LED with red, green, and blue phosphors contains a notable cavity in the cyan region of the visible spectrum (480–520 nm), which reduces the color quality produced by these lights. Here, we report a new bright blue-cyan-emitting phosphor, NaMgBO₃:Ce³⁺, which bridges the gap. Rietveld refinements verify the rare-earth substitution while ab initio calculations prove that Ce³⁺ occupies the Na⁺ sites. NaMgBO₃:Ce³⁺ is excited by a broad range of near-UV light sources and produces a blue-cyan emission with a high (internal) quantum efficiency, minimal thermal degradation, and zero-chromaticity drift at elevated temperatures. Fabricating a near-UV ($\lambda_{\text{ex}} = 370$ nm) pumped pc-wLED using NaMgBO₃:Ce³⁺ along with commercially available phosphors demonstrates a well-distributed warm white light with a high color-rendering index (R_a) of 91 and a low correlated color temperature (CCT) of 3645 K. Closing the cyan cavity with NaMgBO₃:Ce³⁺ is ideal for generating a pleasant, full-spectrum warm white light.



INTRODUCTION

Phosphor-converted white light-emitting diodes (pc-wLEDs) have numerous advantages compared to incandescent or compact fluorescent light bulbs, including higher luminous efficacy, longer operating lifetimes, and environmentally benign components in the LED bulbs.^{1–3} As a result, these devices are rapidly becoming an indispensable lighting source for daily life. The most common white LED-based light uses a blue InGaN LED chip coated with a yellow-emitting phosphor like Y₃Al₅O₁₂:Ce³⁺ (YAG:Ce³⁺). Although this combination produces a functional white light, this approach suffers from poor color-rendering ($R_a < 75$) and high correlated color temperatures (CCT > 4500 K) due to the lack of a red spectral component.^{4,5} One approach to improve the color-rendering index (CRI) and CCT is to fabricate a device using a blue LED chip coated with a green-emitting phosphor, such as β -SiAlON:Eu²⁺, and a red-emitting phosphor, such as CaAlSiN₃:Eu²⁺.^{6,7} This method also generates a reasonable white light; however, it is difficult to realize a full-spectrum emission from this scheme because it creates a gap in the 480–520 nm region of the visible spectrum, also called the “cyan cavity.” Moreover, the bright blue light produced by the LED chip has been widely suggested to have a negative impact on our circadian rhythm.^{8–10} Therefore, a push toward human-centric lighting with a full-spectrum emission and reduced blue LED contribution is currently a major research focus.

Fabricating a lighting device that uses a near-UV LED (360–420 nm) as the excitation source with three phosphors (blue, green, and red-emitting materials) has proven to be a

viable method for diminishing the blue light while still producing a high-quality warm white light.^{11–14} The limitation of this approach, however, is that combining the higher energy near-UV LED chips with the current commercial phosphors still produces the cyan cavity.¹⁵ This gap prevents these devices from achieving a true full-spectrum white light that resembles sunlight and can also negatively influence the circadian rhythm.¹⁶ One solution is to replace the blue-emitting phosphor, which is usually BaMgAl₁₀O₁₇:Eu²⁺, with a different near-UV excited broadband phosphor that covers the blue and cyan regions of the electroluminescence spectrum.^{17,18} Beyond producing a blue-cyan emission, the requirements for such a desirable phosphor also includes possessing a high photoluminescence quantum yield (PLQY), indicating high efficiency and outstanding thermal stability such that a majority of the phosphor’s emission intensity remains at even elevated temperatures.

In recent years, borate phosphors have regained considerable attention as possible phosphor hosts owing to their easily accessible synthesis conditions, excellent chemical and physical stability, and low raw material cost. One of the most intriguing borates reported is a family of efficient orthoborate phosphors, doping the classical CaAlSiN₃ composition type, i.e., 1-1-1-3

Received: November 15, 2019

Revised: December 28, 2019

Published: December 30, 2019

composition type, with the general formula $\text{NaMgBO}_3:\text{Ce}^{3+}$ ($M = \text{Ca, Sr, Ba}$).^{19–21} $\text{NaCaBO}_3:\text{Ce}^{3+}$ crystallizes in the orthorhombic crystal system (space group $Pmmn$), in which Ce^{3+} partially substitutes Ca^{2+} sites, whereas $\text{NaSrBO}_3:\text{Ce}^{3+}$ and $\text{NaBaBO}_3:\text{Ce}^{3+}$ both crystallize in the monoclinic crystal system but with different space groups ($P21/c$ and $C2/m$, respectively). These phosphors all show an efficient (PLQY > 65%) broadband blue emission with the emission spectrum occurring in the near-UV to the blue region with a peak at ~ 425 nm. Unfortunately, these blue-emitting phosphors do not perform well at elevated temperatures with more than 50% integrated emission intensity lost by 423 K, which is the temperature that is considered as the normal operating temperature for most LED packages.

Another orthoborate in the 1-1-1-3 composition type is NaMgBO_3 , which crystallizes in the monoclinic space group $C2/c$,²² has never been systematically investigated as a phosphor for white lighting. This compound is particularly fascinating considering Ce^{3+} could occupy the significantly smaller cation sites, i.e., Na^+ or Mg^{2+} , causing the emission spectrum to shift to longer wavelength region than $\text{NaMgBO}_3:\text{Ce}^{3+}$ ($M = \text{Ca, Sr, Ba}$) compounds following crystal field splitting arguments.²³ Provided the emission peak remains broad in $\text{NaMgBO}_3:\text{Ce}^{3+}$, it may be possible to produce a phosphor that covers the cyan and blue regions simultaneously. Moreover, the compact and symmetric atomic arrangements in $\text{NaMgBO}_3:\text{Ce}^{3+}$ are also expected to result in the improvement in efficiency and thermal stability.^{24,25}

In this work, we investigate $\text{NaMgBO}_3:\text{Ce}^{3+}$ using high-temperature solid-state synthesis, and characterize the product using synchrotron X-ray powder diffraction and electron microscopy. Rietveld refinements and ab initio calculations confirmed Ce^{3+} occupation on the Na^+ site. The detailed insight into the photoluminescence properties of $\text{NaMgBO}_3:\text{Ce}^{3+}$ shows a bright blue-cyan emission peaking at ~ 480 nm under 370 nm excitation with a high PLQY of 93%. Temperature-dependent photoluminescence emission spectra indicate weak thermal quenching, where more than 90% of the integrated emission intensity remains at 423 K, and zero-chromaticity drift as a function of temperature. Evaluating temperature-dependent X-ray diffraction confirms that the zero-chromaticity drift originates from the negligible impact of temperature on the average local structure of the Ce^{3+} sites. Finally, a prototype pc-wLED device employing this new blue-cyan-emitting phosphor generates a full-spectrum white light with an excellent CRI ($R_a > 90$) and low CCT (3645 K), indicating the potential application of this phosphor in energy-efficient and full-spectrum warm white lighting.

EXPERIMENTAL SECTION

Synthesis. $\text{NaMgBO}_3:x\text{Ce}^{3+}$ ($x = 0, 0.001, 0.005, 0.01, 0.015, \text{ and } 0.02$) were prepared by conventional high-temperature solid-state reaction using NaHCO_3 (Aldrich, 99.95%), $4\text{MgCO}_3\cdot\text{Mg}(\text{OH})_2\cdot 5\text{H}_2\text{O}$ (Aldrich, 99.9%), H_3BO_3 (Aldrich, 99.5%), and CeO_2 (Aldrich, 99.995%) as the starting materials. The powders were weighed out according to the required stoichiometric ratio with a 3% excess of H_3BO_3 added as flux, and 1–2% excess of NaHCO_3 included to compensate for potential evaporation during synthesis. The powder was ground using an agate mortar and pestle and the homogeneous mixtures were placed in an alumina crucible. The mixtures were heated to 873 K with a heating rate of 2 K/min and held at this temperature for 8 h to decompose H_3BO_3 and $4\text{MgCO}_3\cdot\text{Mg}(\text{OH})_2\cdot 5\text{H}_2\text{O}$. The powder was reground and heated to 1043 K with a heating rate of 2 K/min for 8 h under a reducing atmosphere (5% H_2 /

95% N_2). The final products were ground into a fine powder using an agate mortar and pestle and then washed with hot deionized water to remove the minor sodium and boron oxide impurities. Lastly, the products were dried at 443 K for 30 min before conducting characterizations.

Characterization. Powder X-ray diffractograms (X'Pert3 PANalytical; $\text{Cu K}\alpha$, $\lambda = 1.5406$ Å) were collected to confirm phase purity with the temperature-dependent X-ray diffractograms collected using an Anton-Paar TTK450 chamber. The synchrotron X-ray powder diffraction data were collected at 298 K using beamline 11-BM at the Advanced Photon Source with a calibrated wavelength of 0.412835 Å.²⁶ The Rietveld and Le Bail profile refinements were performed with the General Structure Analysis System (GSAS) software and the EXPGUI interface.^{27,28} The scanning electron microscopy (SEM) images and energy-dispersive X-ray spectroscopy (EDS) elemental mappings were collected on a Hitachi-S4800 (Japan). The high-resolution transmission electron microscopy (HRTEM) images were acquired by using a TecnaiG2F30 (FEI) microscope with an accelerating voltage of 300 kV. The room temperature and temperature-dependent photoluminescent spectra were recorded on a Horiba Fluoromax-4 fluorescence spectrophotometer with a 150 W xenon arc lamp for excitation and a Janis cryostat (VPP-100) to control the temperature between 80 and 500 K. The internal PLQY was determined by placing the samples encapsulated in the silicone resin (GE Silicones, RTV615) inside a Spectralon-coated integrating sphere (150 mm diameter, Labsphere) with the PLQY values calculated out by the method of De Mello et al.²⁹ The thermoluminescence (TL) curves were collected by a thermoluminescence meter (SL08-L, Guangzhou-Radiation Science and Technology Co. Ltd.) with the heating rate of 1 K/s after being excited ($\lambda_{\text{ex}} = 254$ nm) for 10 min. The fabrication of a pc-wLED device involved the addition of commercial green-emitting $\beta\text{-SiAlON}:\text{Eu}^{2+}$, red-emitting $\text{Sr}_2\text{Si}_5\text{N}_8:\text{Eu}^{2+}$, and the blue-cyan-emitting $\text{NaMgBO}_3:0.1\text{Ce}^{3+}$ phosphor described here, in the silicone resin. This mixture was then coated on a $\lambda_{\text{ex}} = 370$ nm emitting UV-LED (Thorlabs, LED370E). The electroluminescence spectrum, CRI, and CCT of the pc-LED device were measured under a forward bias of 20 mA using an AvaFast Fiber Optic VIS/NIR spectrometer coupled to a 50 mm integrating sphere.

Computation. The crystal structure of NaMgBO_3 was optimized using the Vienna ab initio simulation package (VASP), which is a plane-wave pseudopotential total energy package based on density functional theory (DFT).³⁰ The structures were relaxed with electronic convergence criteria of 1×10^{-5} eV and atomic convergence criteria of 0.01 eV/Å. A cutoff energy of 500 eV was used for the basis set of the plane waves, and an $8 \times 6 \times 8$ Γ -centered Monkhorst–Pack k -point grid was used to sample the first Brillouin zone. The PBE exchange–correlation functional was employed for structure optimization. The defect calculations were examined by calculating the formation energy of different defect models using the PBE0 hybrid functional.³¹

RESULTS AND DISCUSSION

Crystal Structure and Rare-Earth Site Occupation.

The phase purity of $\text{NaMgBO}_3:x\text{Ce}^{3+}$ ($x = 0, 0.001, 0.005, 0.01, 0.015, \text{ and } 0.02$) was first analyzed by powder X-ray diffraction, shown in Figure S1. The diffraction peaks index to the monoclinic space group $C2/c$, which is in agreement with the reported crystal structure.²² To obtain accurate structural data, Rietveld refinements of high-resolution synchrotron X-ray diffractograms for NaMgBO_3 and $\text{NaMgBO}_3:0.01\text{Ce}^{3+}$ were performed, as plotted in Figures 1a and S2, respectively. The results of the refinements are provided in Table 1, and the refined atomic coordinates are provided in Table S1. These data support the phase purity and confirm the crystal structure. The morphology of $\text{NaMgBO}_3:0.01\text{Ce}^{3+}$ was also examined using scanning electron microscopy (SEM), shown in Figure 1b. The micrographs reveal that the particles have an irregular

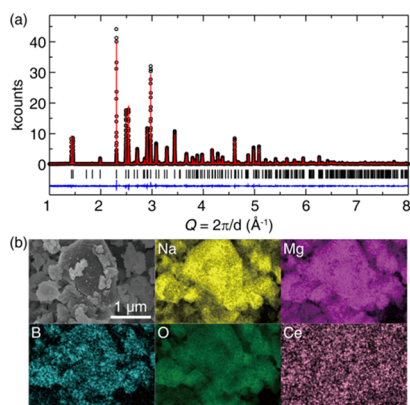


Figure 1. (a) Rietveld refinement of high-resolution synchrotron X-ray diffraction patterns of NaMgBO₃. The measured data are represented by black circles, the refinement fit is in red, and the difference curve is in blue; (b) scanning electron microscopy (SEM) and energy-dispersive X-ray (EDS) mapping of NaMgBO₃:0.01Ce³⁺.

Table 1. Rietveld Refinement Data of NaMgBO₃ and NaMgBO₃:0.01Ce³⁺

composition	NaMgBO ₃	NaMgBO ₃ :0.01Ce ³⁺
radiation type; λ (Å)	synchrotron; 0.412835	synchrotron; 0.412835
Q range (Å ⁻¹)	1.00–8.00	1.00–8.00
temperature (K)	298	298
space group; Z	C2/c; 4	C2/c; 4
a (Å)	5.01271(4)	5.01534(0)
b (Å)	8.80173(5)	8.80294(6)
c (Å)	5.52858(0)	5.53463(6)
β (°)	99.73(6)	99.66(2)
unit cell volume (Å ³)	240.41(1)	240.88(7)
R _p	0.0690	0.0830
R _{wp}	0.0860	0.1155
χ ²	2.343	3.623

morphology with a wide size distribution as prepared with a size that is generally <3 μm. Further optimizing the synthetic process, such as extending sintering time, may lead to a much better crystalline morphology and larger particle size (shown as Figure S3). Mapping the elemental distribution using energy-dispersive X-ray spectrometry (EDS) shows that only the loaded starting elements are present in the product, and there is no contamination from the synthesis, i.e., aluminum from the crucible. Further, these data verify that Na, Mg, B, O, and Ce are uniformly distributed in the region examined.

NaMgBO₃ is isostructural with β-K₂CO₃ and can be described as a cosubstitution (Figure S4) of the octahedral K(1)O₆ → MgO₆, trigonal CO₃ → BO₃, and coplanar hexagonal K(2)O₆ units evolving into O–NaO₆–O (NaO₈) through additional connections with two oxygen ions from the upper and lower layers of the BO₃ units. To illustrate this crystal structure, a 2 × 2 × 1 supercell of NaMgBO₃ is depicted in Figure 2a–c. As shown in Figure 2a, NaMgBO₃ can be divided into two layers defined here as *m* and *n*. The *n* layer can be obtained by rotating 180° along the *c* axis from the *m* layer, and the two layers are connected by [MgO₆] octahedron. Taking the *m* layer and viewing it in the *c* direction, plotted in Figure 2c, shows a slightly puckered hexagonal network of trigonal planar [BO₃] units that are stitched together by Mg²⁺ ions. The Na⁺ ions are located at the center of a dodecagon composed of B–O and Mg–O bonds and are separated by

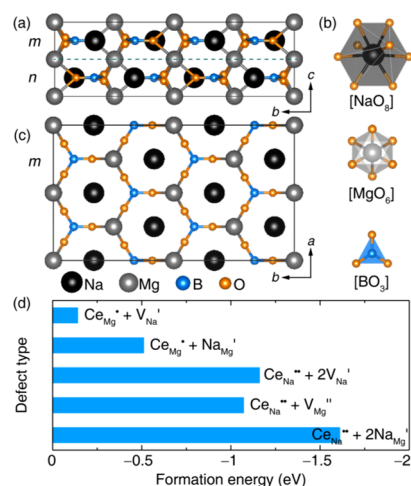


Figure 2. (a) A 2 × 2 × 1 supercell of NaMgBO₃ viewed from the *a* direction. (b) Coordination environments of cations in NaMgBO₃; (c) atomic arrangement in the *m* layer viewed from the *c* direction; (d) calculated relative defect formation energies using the hybrid functional.

[BO₃] units between upper and lower layers. Once Ce³⁺ is incorporated in the crystal structure, the highly condensed crystal structure backbone should give rise to a rigid structure that is ideal for a phosphor host.

Comparing the refined lattice parameters of unsubstituted NaMgBO₃ with NaMgBO₃:Ce³⁺ reveals the lattice parameters of the structure expand upon Ce³⁺ substitution. This increase is also observed by high-resolution transmission electron microscopy (HRTEM) where the micrographs show well-resolved lattice fringes with an interplanar distance of 0.2157 nm for the (220) plane of NaMgBO₃:Ce³⁺, which is slightly larger than that in NaMgBO₃ (0.2154 nm), as shown in Figure S5. Comparing the ionic radius of 6-coordinate Ce³⁺ (*r*_{6-coord.} = 1.01 Å) with Mg²⁺ (*r*_{6-coord.} = 0.72 Å) suggests that it is unlikely for the rare-earth ion to replace Mg²⁺ because their radius difference is as high as ≈40%, which is beyond the limits of the Hume-Rothery rules for atomic substitution.^{32,33} The lattice expansion is, therefore, expected to be the result of Ce³⁺ (*r*_{8-coord.} = 1.143 Å) replacing Na⁺ (*r*_{8-coord.} = 1.18 Å).³³

To further confirm the site preference of Ce³⁺ and investigate the likely defects owing to the aliovalent substitution in NaMgBO₃, DFT calculations employing the PBE0 hybrid functional were performed to evaluate the formation energy of different Ce³⁺ site substitution patterns. More calculation details regarding the structure optimization, band structure, and absorption spectrum are provided in Figure S6. Within this crystal structure, there are five possible types of neutral defects that can occur, including Ce_{Mg}[•] + V_{Na}['] (Ce³⁺ entering into Mg²⁺ site and a vacancy on the Na⁺ site), Ce_{Mg}[•] + Na_{Mg}['] (Ce³⁺ entering into Mg²⁺ site and additional Na⁺ entering into another Mg²⁺ site), Ce_{Na}^{••} + 2V_{Na}['] (Ce³⁺ entering into Na⁺ site and two vacancies on the Na⁺ site), Ce_{Na}^{••} + V_{Mg}^{''} (Ce³⁺ entering into Na⁺ site and a vacancy on the Mg²⁺ site), and Ce_{Na}^{••} + 2Na_{Mg}['] (Ce³⁺ entering into Na⁺ site and two additional Na⁺ entering into two Mg²⁺ site). The calculated relative defect formation energies using the hybrid functional are provided in Figure 2d and Table S2. The defect formation energies for all permutations of Ce³⁺ entering the Na⁺ site are much lower than when entering the Mg²⁺ site. Additionally, Ce³⁺ entering the Na⁺ site with two additional

Na⁺ entering into two Mg²⁺ sites has the lowest defects formation energy. Moreover, comparing the lattice parameters of the DFT optimized crystal structure containing the Ce_{Na}^{••} + 2Na_{Mg}['] defect with the unsubstituted NaMgBO₃ unit cell shows a notable expansion (Table S3), which is also in agreement with the experimental results. These results provide clear evidence that Ce³⁺ enters into the Na⁺ site and that Ce_{Na}^{••} + 2Na_{Mg}['] is the favorable (neutral) defect that occurs upon rare-earth substitution.

Photoluminescence Properties. The photoluminescent excitation and emission spectra of NaMgBO₃:0.01Ce³⁺ are presented in Figure 3a. This phosphor has an excitation

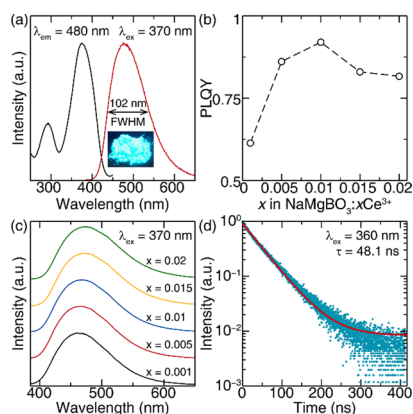


Figure 3. (a) Excitation and emission spectra of NaMgBO₃:0.01Ce³⁺ at room temperature, inset shows the digital photograph of NaMgBO₃:0.01Ce³⁺ under 365 nm lamp. (b) Room temperature photoluminescence quantum yield (PLQY) of NaMgBO₃:xCe³⁺ ($x = 0.001, 0.005, 0.01, 0.015,$ and 0.02) under 370 nm excitation. (c) Emission spectra of NaMgBO₃:xCe³⁺ ($x = 0.001, 0.005, 0.01, 0.015,$ and 0.02) phosphors under 370 nm excitation at room temperature. (d) Room temperature photoluminescence lifetime decay curve of NaMgBO₃:0.01Ce³⁺ phosphor excited at 360 nm. The fit is shown in the red line.

spectrum (monitored at $\lambda_{em} = 480$ nm) that spans from 250 to 430 nm with two peaks centered at 294 and 376 nm which are ascribed to electronic transitions from the 4f ground state to different 5d orbitals of the Ce³⁺ ion. Such a broad near-UV excitation band demonstrates the potential for application with a range of near-UV pumped pc-LEDs. Exciting NaMgBO₃:Ce³⁺ at 370 nm produces a very bright blue-cyan emission (as shown in the inset of Figure 3a) with a broad full width at half-maximum (FWHM) of 102 nm (4516 cm^{-1}) that covers the blue and cyan regions. As shown in Figure 3b, varying the rare-earth concentration from 0.1 to 2% indicates that 1% Ce³⁺ substitution has the highest PLQY reaching 93% ($\lambda_{ex} = 370$ nm) at room temperature. Increasing the Ce³⁺ concentration to 1.5% and then 2% causes a drop in PLQY. This concentration quenching is likely a result of energy transfer between two nearest activator ions, such as exchange interactions, radiation reabsorption, or multipole–multipole interactions.³⁴ Out of these possible mechanisms, the exchange interactions and reabsorption mechanisms can be excluded because the spectral overlap between excitation and emission spectra is negligible, and the calculated critical distance, R_0 is 22 Å, which is much too long for quenching (>5 Å).³⁵ As a result, the quenching is likely owing to multipole–multipole interactions. Following Dexter's theory,³⁶ the concentration quenching mechanism is determined more specifically to be

dipole–dipole (d–d) interactions through linear fitting the relationship of $\lg(I/x)$ vs $\lg(x)$ (Figure S7).

The emission peak wavelength shifts from 472 to 483 nm (Figure 3c) and exhibits slight broadening with increasing Ce³⁺ concentration. This shift in emission spectra stems from a gradual increase in the crystal field strength caused by larger Ce³⁺ substituting for the smaller Na⁺. As more Ce³⁺ is loaded into this rigid crystal structure, there is a shortening of the mean bond length in the Ce³⁺ polyhedra, which leads to an enhancement in the crystal field surrounding the Ce³⁺ and thus a larger crystal field splitting of the 5d orbitals of Ce³⁺. Generally, the broadening of emission spectra can be ascribed to the gradually enhanced energy transfer from higher energy luminescence center to lower energy luminescence center with an increase in the Ce³⁺ concentration.³⁷ However, in this phosphor, due to the increasing amount of antisite defects with the increase of Ce³⁺ doping concentration, the local structure around Ce³⁺ may also be slightly distorted resulting in the observed spectral broadening,³⁸ although it is not possible to determine the exact mechanism.

Probing the optical properties of NaMgBO₃:0.01Ce³⁺ by measuring the time-resolved photoluminescence decay curve under 360 nm excitation at room temperature (Figure 3d), shows that the decay curve can be well fitted by a single exponential function. This analysis confirms the presence of a single crystallographically independent luminescence center with a lifetime of 48.3 ns for NaMgBO₃:0.01Ce³⁺, which is shorter than YAG:Ce³⁺ (~65 ns) but slightly longer than La₃Si₆N₁₁:Ce³⁺ (~42 ns).^{37,39} Interestingly, increasing the Ce³⁺ concentration shows that the decay curves gradually deviate from single exponential function (Figure S8), which further suggests that there is a change in the local structure of the Ce³⁺ sites in this material.

Outstanding thermal performance of NaMgBO₃:Ce³⁺ is essential for practical applications because LED-based lights operate at temperatures up to 423 K.⁴⁰ Consequently, the thermal quenching and chromaticity stability of the phosphor was evaluated. The temperature-dependent emission spectra of NaMgBO₃:0.01Ce³⁺ were collected from 80 to 500 K ($\lambda_{ex} = 370$ nm). The raw spectra are provided in Figure S9, and the contour plot of the spectra and normalized integrated (peak) intensity as a function of temperature are plotted in Figure 4a and b, respectively. Obviously, both the normalized integrated

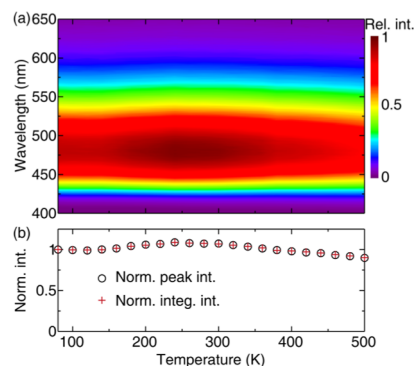


Figure 4. (a) Contour plot of the emission spectra of NaMgBO₃:0.01Ce³⁺ phosphor excited at 370 nm as a function of temperature. (b) Normalized integrated intensity of the emission spectra (norm. integ. int.) and normalized intensity of the emission peak (norm. peak int.) as a function of temperature.

emission intensity and the normalized peak intensity first slightly increases with increasing temperature achieving a maximum at 240 K, followed by the expected decrease as the phosphor begins to thermally quench. Generally, the increase of emission intensity with increasing temperature is due to the release of electrons from defect-induced trap states. Thus, thermoluminescence measurements on $\text{NaMgBO}_3:\text{Ce}^{3+}$ were collected from 300 to 680 K to corroborate the presence of trap states. These data, presented in Figure S10, were analyzed by decomposing the thermoluminescence spectrum using three Gaussian curves centered at 485, 491, and 538 K. Estimating the trap depths following the approximate relationship $E_T = T/500$,⁴¹ where T is temperature, suggests the traps occur at ~ 0.97 , ~ 0.98 , and ~ 1.08 eV, respectively. The presence of trap states in this phosphor supports the energetically favorable formation of defects as determined by DFT. Even with the presence of these defects, they do not significantly influence the temperature-dependent optical properties. The normalized integrated emission intensity and the normalized peak intensity retain 96% of the low-temperature emission spectrum at 420 K and 90% at 500 K. These results reveal that minimal thermal degradation occurs for $\text{NaMgBO}_3:\text{Ce}^{3+}$.

The origin of the weak thermal degradation can be ascribed to multiple sources that each mitigates a different thermal quenching mechanism. For example, the relatively wide band gap ($E_{\text{g,HSE}} = 5.5$ eV) of host crystal structure can prevent photo or thermal ionization, the high structural rigidity (Debye temperature $\Theta_D = 563$ K) of host can reduce nonradiative relaxation pathways, the low substitution concentration (1 mol %) of Ce^{3+} can prevent energy-transfer quenching, and finally, the similar ionic radii of 8-coordinate Ce^{3+} ($r_{8\text{-coord.}} = 1.143$ Å) and Na^+ ($r_{8\text{-coord.}} = 1.18$ Å) minimizes the local distortions of the host crystal structure that can induce additional defects.^{42,43}

Further analysis of the temperature-dependent data by normalizing the temperature-dependent emission spectra indicates no perceptible spectral shift or change in the emission peak's FWHM when the temperature increased from 80 to 500 K (Figure 5a). This negligible chromaticity drift is rather uncommon in rare-earth substituted phosphors. To explore the fundamental mechanism leading to the zero-chromaticity drift, temperature-dependent powder X-ray diffractions of $\text{NaMgBO}_3:0.01\text{Ce}^{3+}$ were collected from 298 to 523 K (Figure 5b). The unit cell volumes obtained from the Le Bail refinement method shows the anticipated thermal expansion with increasing temperature (Figure 5c). However, analyzing the Miller indices of specific diffraction peaks shows some noteworthy trends. The interplanar distances of the (200) plane, which consist of Na, Mg, B, and O atoms, and the (020) plane, which is composed of Mg atoms, shown in Figure 5d, both remain nearly unchanged at all temperatures. This is different from the interplanar distance of the (002) plane that is composed of Mg atoms that shows a shift as a function of temperature. Taken in combination, it is clear the atomic arrangement is very compact and shows less influence on the planes parallel to the ab plane, whereas the distances along the c axis expand. This change allows the six shorter Na–O bonds of NaO_8 on the planes parallel to ab plane to remain unchanged, and the two longer Na–O bonds connected with $[\text{BO}_3]$ to slightly increase. This insignificant change in the coordination environment of the Na^+ site suggests robust site symmetry for this phosphor, which is likely the source of the

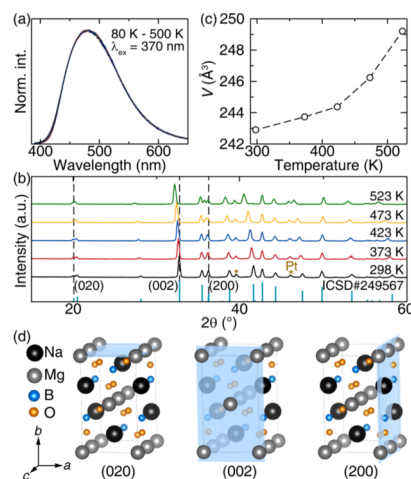


Figure 5. (a) Normalized temperature-dependent emission spectra of $\text{NaMgBO}_3:0.01\text{Ce}^{3+}$ measured from 80 to 500 K using 370 nm excitation. (b) Temperature-dependent powder X-ray diffraction patterns collected from 298 to 523 K. Diffraction peaks marked as yellow stars are derived from Pt sample holder. (c) Unit cell volume (V) from Le Bail refinements as a function of temperature. (d) Structure of NaMgBO_3 with (020), (002), and (200) planes highlighted in blue.

zero-chromaticity drift and is likely also related to the thermal stability, in general.

Application of Full-Spectrum pc-wLEDs. The potential of the novel $\text{NaMgBO}_3:\text{Ce}^{3+}$ blue-cyan-emitting phosphor was finally evaluated to demonstrate its potential in full-spectrum warm white lighting applications. A prototype pc-LED device was fabricated by combining a near-UV LED chip ($\lambda_{\text{ex}} = 370$ nm) with a mixture of the blue-cyan-emitting $\text{NaMgBO}_3:\text{Ce}^{3+}$ phosphor developed here, along with a green-emitting $\beta\text{-SiAlON}:\text{Eu}^{2+}$ phosphor, and a red-emitting $\text{Sr}_2\text{Si}_5\text{N}_8:\text{Eu}^{2+}$ phosphor and driven by 20 mA to yield the corresponding photoluminescence spectrum (Figure 6a). To show the capability of $\text{NaMgBO}_3:\text{Ce}^{3+}$ to close the cyan gap, blue-emitting $\text{BaMgAl}_{10}\text{O}_{17}:\text{Eu}^{2+}$ was also mixed with $\beta\text{-SiAlON}:\text{Eu}^{2+}$ and $\text{Sr}_2\text{Si}_5\text{N}_8:\text{Eu}^{2+}$ to fabricate a similar device. The spectrum generated with the $\text{NaMgBO}_3:\text{Ce}^{3+}$ -containing device exhibits a continuous broadband emission, covering

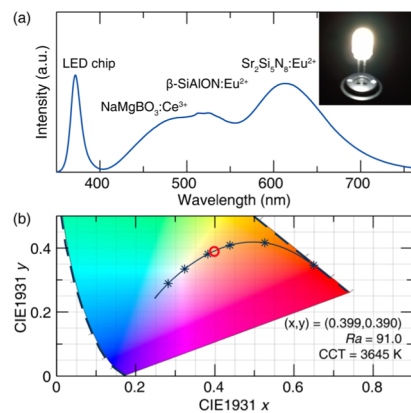


Figure 6. (a) Emission spectrum of a white LED fabricated by $\text{NaMgBO}_3:0.01\text{Ce}^{3+}$, $\beta\text{-SiAlON}:\text{Eu}^{2+}$, $\text{Sr}_2\text{Si}_5\text{N}_8:\text{Eu}^{2+}$, and a 370 nm LED chip; the inset is the photograph of the white LED under a forward bias of 20 mA. (b) The CIE coordinates of the fabricated white LED.

the whole visible region without the cyan cavity that is present in the $\text{BaMgAl}_{10}\text{O}_{17}:\text{Eu}^{2+}$ -containing device, as shown in Figure S11. In addition, as shown in Figure 6b, the white light generated from the $\text{NaMgBO}_3:\text{Ce}^{3+}$ -fabricated device shows CIE coordinates of (0.399, 0.390), a CCT of 3645 K, and an R_a of 91.0, indicating the production of warm white light with outstanding color quality. These results express the suitability of the blue-cyan-emitting $\text{NaMgBO}_3:\text{Ce}^{3+}$ for covering the cavity in the cyan region and the capability of this phosphor in the realization of a full-spectrum pc-wLED.

CONCLUSIONS

In summary, a highly efficient and thermally stable blue-cyan-emitting $\text{NaMgBO}_3:\text{Ce}^{3+}$ phosphor with monoclinic $\beta\text{-K}_2\text{CO}_3$ structure type has been identified. The site occupancy of Ce^{3+} was verified to be on the Na^+ site, and this aliovalent substitution caused antisite defects in the crystal structure to balance the charge. This phosphor can be excited using a near-UV ($\lambda_{\text{ex}} = 370 \text{ nm}$) LED to produce a broadband blue-cyan emission with a high PLQY of 93%, minimal thermal quenching, and zero-chromaticity drift at elevated temperatures. Temperature-dependent XRD measurements indicate that this zero-chromaticity drift stems from the negligible change in the crystal structure around the Ce^{3+} site. Furthermore, fabricating a pc-wLED device by blending this blue-cyan-emitting phosphor with green-emitting and red-emitting phosphors confirms the ability to close the cyan cavity and cover the entire electromagnetic spectrum, in turn, generating a high CRI and low CCT warm white light. These data provide substantial evidence for the vital role this new blue-cyan-emitting $\text{NaMgBO}_3:\text{Ce}^{3+}$ phosphor can make in near-UV-pumped full-spectrum pc-wLEDs.

ASSOCIATED CONTENT

Supporting Information

The Supporting Information is available free of charge at <https://pubs.acs.org/doi/10.1021/acs.chemmater.9b04739>.

Computation procedures, electronic properties, Rietveld refinements results, XRD, SEM, HRTEM, TL curve, temperature-dependent emission spectra, and electroluminescence spectrum of devices (PDF)

AUTHOR INFORMATION

Corresponding Authors

Weiren Zhao – Guangdong University of Technology, Guangzhou, China; Email: zwren123@126.com

Jakoah Brgoch – University of Houston, Houston, Texas; orcid.org/0000-0002-1406-1352; Email: jbrgoch@uh.edu

Other Authors

Jiyou Zhong – Guangdong University of Technology, Guangzhou, China; orcid.org/0000-0003-2817-6617

Ya Zhuo – University of Houston, Houston, Texas; orcid.org/0000-0003-2554-498X

Shruti Hariyani – University of Houston, Houston, Texas; orcid.org/0000-0002-4707-8863

Jun Wen – Anqing Normal University, Anqing, China; orcid.org/0000-0002-0490-3536

Complete contact information is available at:

<https://pubs.acs.org/doi/10.1021/acs.chemmater.9b04739>

Author Contributions

J.Z. and Y.Z. contributed equally to this work.

Notes

The authors declare no competing financial interest.

ACKNOWLEDGMENTS

The authors thank the National Natural Science Foundation of China (Nos. 51702057 and 11604002), the National Science Foundation (DMR 18-47701 and CER 19-11311), and the University of Houston Division of Research and the Grant to Enhance and Advance Research for funding this research. This research used the Maxwell/Opuntia/Sabine cluster(s) operated by the University of Houston and the Research Computing Data Core (RCDC). Support for this work was also provided by resources of the uHPC cluster managed by the University of Houston and acquired through NSF Award Number 15-31814. This work used the resources available through the 11-BM beamline at the Advanced Photon Source, an Office of Science User Facility operated for the U.S. Department of Energy (DOE) Office of Science by Argonne National Laboratory, under Contract No. DE-AC02-06CH11357.

REFERENCES

- (1) Nanishi, Y. Nobel Prize in Physics: The Birth of the Blue LED. *Nat. Photonics* **2014**, *8*, 884–886.
- (2) Pimputkar, S.; Speck, J. S.; Denbaars, S. P.; Nakamura, S. Prospects for LED Lighting. *Nat. Photonics* **2009**, *3*, 180–182.
- (3) Pust, P.; Schmidt, P. J.; Schnick, W. A Revolution in Lighting. *Nat. Mater.* **2015**, *14*, 454–458.
- (4) George, N. C.; Denault, K. A.; Seshadri, R. Phosphors for Solid-State White Lighting. *Annu. Rev. Mater. Res.* **2013**, *43*, 481–501.
- (5) Im, W. Bin.; George, N.; Kurzman, J.; Brinkley, S.; Mikhailovsky, A.; Hu, J.; Chmelka, B. F.; Denbaars, S. P.; Seshadri, R. Efficient and Color-Tunable Oxyfluoride Solid Solution Phosphors for Solid-State White Lighting. *Adv. Mater.* **2011**, *23*, 2300–2305.
- (6) Uheda, K.; Hirosaki, N.; Yamamoto, Y.; Naito, A.; Nakajima, T.; Yamamoto, H. Luminescence Properties of a Red Phosphor, $\text{CaAlSiN}_3:\text{Eu}^{2+}$, for White Light-Emitting Diodes. *Electrochem. Solid-State Lett.* **2006**, *9*, H22–H25.
- (7) Xie, R. J.; Hirosaki, N.; Li, H. L.; Li, Y. Q.; Mitomo, M. Synthesis and Photoluminescence Properties of $\beta\text{-Sialon}:\text{Eu}^{2+}$ ($\text{Si}_{6-z}\text{Al}_z\text{O}_7\text{N}_{8-z}:\text{Eu}^{2+}$). *J. Electrochem. Soc.* **2007**, *154*, J314–J319.
- (8) Bellia, L.; Bisegna, F.; Spada, G. Lighting in Indoor Environments: Visual and Non-Visual Effects of Light Sources with Different Spectral Power Distributions. *Build. Environ.* **2011**, *46*, 1984–1992.
- (9) Pauley, S. M. Lighting for the Human Circadian Clock: Recent Research Indicates That Lighting Has Become a Public Health Issue. *Med. Hypotheses* **2004**, *63*, 588–596.
- (10) Oh, J. H.; Yang, S. J.; Do, Y. R. Healthy, Natural, Efficient and Tunable Lighting: Four-Package White LEDs for Optimizing the Circadian Effect, Color Quality and Vision Performance. *Light Sci. Appl.* **2014**, *3*, No. e141.
- (11) Wan, J.; Liu, Q.; Zhou, Z.; Xie, R. J. $\text{Y}_2\text{Si}_4\text{N}_6\text{C}:\text{Ce}^{3+}$ Carbide Nitride Green-Yellow Phosphors: Novel Synthesis, Photoluminescence Properties, and Applications. *J. Mater. Chem. C* **2017**, *5*, 6061–6070.
- (12) Ding, X.; Zhu, G.; Geng, W.; Wang, Q.; Wang, Y. Rare-Earth-Free High-Efficiency Narrow-Band Red-Emitting $\text{Mg}_3\text{Ga}_2\text{GeO}_8:\text{Mn}^{4+}$ Phosphor Excited by Near-UV Light for White-Light-Emitting Diodes. *Inorg. Chem.* **2016**, *55*, 154–162.
- (13) Liao, H.; Zhao, M.; Molokeev, M. S.; Liu, Q.; Xia, Z. Learning from a Mineral Structure toward an Ultra-Narrow-Band Blue-Emitting Silicate Phosphor $\text{RbNa}_3(\text{Li}_3\text{SiO}_4)_4:\text{Eu}^{2+}$. *Angew. Chem.* **2018**, *130*, 11902–11905.

- (14) Sheu, J. K.; Chang, S. J.; Kuo, C. H.; Su, Y. K.; Wu, L. W.; Lin, Y. C.; Lai, W. C.; Tsai, J. M.; Chi, G. C.; Wu, R. K. White-Light Emission from near UV InGaN-GaN LED Chip Precoated with Blue/Green/Red Phosphors. *IEEE Photonics Technol. Lett.* **2003**, *15*, 18–20.
- (15) Zhao, M.; Liao, H.; Molokeev, M. S.; Zhou, Y.; Zhang, Q.; Liu, Q.; Xia, Z. Emerging Ultra-Narrow-Band Cyan-Emitting Phosphor for White LEDs with Enhanced Color Rendition. *Light Sci. Appl.* **2019**, *8*, 38.
- (16) Nagare, R.; Rea, M. S.; Plitnick, B.; Figueiro, M. G. Effect of White Light Devoid of “Cyan” Spectrum Radiation on Nighttime Melatonin Suppression Over a 1-h Exposure Duration. *J. Biol. Rhythms* **2019**, *34*, 195–204.
- (17) Fang, M. H.; Ni, C.; Zhang, X.; Tsai, Y. T.; Mahlik, S.; Lazarowska, A.; Grinberg, M.; Sheu, H. S.; Lee, J. F.; Cheng, B. M.; et al. Enhance Color Rendering Index via Full Spectrum Employing the Important Key of Cyan Phosphor. *ACS Appl. Mater. Interfaces* **2016**, *8*, 30677–30682.
- (18) Yan, C.; Liu, Z.; Zhuang, W.; Liu, R.; Xing, X.; Liu, Y.; Chen, G.; Li, Y.; Ma, X. $\text{YScSi}_4\text{N}_6\text{:Ce}^{3+}$ - A Broad Cyan-Emitting Phosphor to Weaken the Cyan Cavity in Full-Spectrum White Light-Emitting Diodes. *Inorg. Chem.* **2017**, *56*, 11087–11095.
- (19) Yi, H.; Wu, L.; Wu, L.; Zhao, L.; Xia, Z.; Zhang, Y.; Kong, Y.; Xu, J. Crystal Structure of High-Temperature Phase β -NaSrBO₃ and Photoluminescence of β -NaSrBO₃:Ce³⁺. *Inorg. Chem.* **2016**, *55*, 6487–6495.
- (20) Zhong, J.; Zhao, W.; Zhuo, Y.; Yan, C.; Wen, J.; Brgoch, J. Understanding the Blue-Emitting Orthoborate Phosphor NaBaBO₃:Ce³⁺ through Experiment and Computation. *J. Mater. Chem. C* **2019**, *7*, 654–662.
- (21) Zhang, X.; Song, J.; Zhou, C.; Zhou, L.; Gong, M. High Efficiency and Broadband Blue-Emitting NaCaBO₃:Ce³⁺ Phosphor for NUV Light-Emitting Diodes. *J. Lumin.* **2014**, *149*, 69–74.
- (22) Wu, L.; Zhang, Y.; Kong, Y. F.; Sun, T. Q.; Xu, J. J.; Chen, X. L. Structure Determination of Novel Orthoborate NaMgBO₃: A Promising Birefringent Crystal. *Inorg. Chem.* **2007**, *46*, 5207–5211.
- (23) Dorenbos, P. Crystal Field Splitting of Lanthanide $4f_n-15d$ -Levels in Inorganic Compounds. *J. Alloys Compd.* **2002**, *341*, 156–159.
- (24) Mikami, M.; Watanabe, H.; Uheda, K.; Shimooka, S.; Shimomura, Y.; Kurushima, T.; Kijima, N. New Phosphors for White LEDs: Material Design Concepts. *IOP Conf. Ser.: Mater. Sci. Eng.* **2009**, *1*, No. 012002.
- (25) Ye, S.; Xiao, F.; Pan, Y. X.; Ma, Y. Y.; Zhang, Q. Y. Phosphors in Phosphor-Converted White Light-Emitting Diodes: Recent Advances in Materials, Techniques and Properties. *Mater. Sci. Eng., R* **2010**, *71*, 1–34.
- (26) Lee, P. L.; Shu, D.; Ramanathan, M.; Preissner, C.; Wang, J.; Beno, M. A.; Von Dreele, R. B.; Ribaud, L.; Kurtz, C.; Antao, S. M.; et al. A Twelve-Analyzer Detector System for High-Resolution Powder Diffraction. *J. Synchrotron Radiat.* **2008**, *15*, 427–432.
- (27) Toby, B. H. EXPGUI, A Graphical User Interface for GSAS. *J. Appl. Crystallogr.* **2001**, *34*, 210–213.
- (28) Larson, A. C.; Von Dreele, R. B. *General Structure Analysis System (GSAS)*; Los Alamos National Laboratory: Los Alamos, New Mexico, 1987.
- (29) De Mello, J. C.; Wittmann, H. F.; Friend, R. H. An Improved Experimental Determination of External Photoluminescence Quantum Efficiency. *Adv. Mater.* **1997**, *9*, 230–232.
- (30) Hafner, J. Ab-Initio Simulations of Materials Using VASP: Density-Functional Theory and Beyond. *J. Comput. Chem.* **2008**, *29*, 2044–2078.
- (31) Heyd, J.; Scuseria, G. E.; Ernzerhof, M. Hybrid Functionals Based on a Screened Coulomb Potential. *J. Chem. Phys.* **2003**, *118*, 8207–8215.
- (32) Hume-Rothery, W.; Powell, H. M. On the Theory of Super-Lattice Structures in Alloys. *Z. Kristallogr. - Cryst. Mater.* **1935**, *91*, 23–47.
- (33) Shannon, R. D. Revised Effective Ionic Radii and Systematic Studies of Interatomic Distances in Halides and Chalcogenides. *Acta Crystallogr., Sect. A* **1976**, *32*, 751–767.
- (34) Zhong, J.; Zhuang, W.; Xing, X.; Liu, R.; Li, Y.; Liu, Y.; Hu, Y. Synthesis, Crystal Structures, and Photoluminescence Properties of Ce³⁺-Doped Ca₂LaZr₂Ga₃O₁₂: New Garnet Green-Emitting Phosphors for White LEDs. *J. Phys. Chem. C* **2015**, *119*, 5562–5569.
- (35) Blasse, G. Energy Transfer between Inequivalent Eu²⁺ Ions. *J. Solid State Chem.* **1986**, *62*, 207–211.
- (36) Dexter, D. L. A Theory of Sensitized Luminescence in Solids. *J. Chem. Phys.* **1953**, *21*, 836–850.
- (37) Bachmann, V.; Ronda, C.; Meijerink, A. Temperature Quenching of Yellow Ce³⁺ Luminescence in YAG:Ce. *Chem. Mater.* **2009**, *21*, 2077–2084.
- (38) Zhong, J.; Zhuang, W.; Xing, X.; Liu, R.; Li, Y.; Zheng, Y.; Hu, Y.; Xu, H. Synthesis, Structure and Luminescence Properties of New Blue-Green-Emitting Garnet-Type Ca₂Zr₂SiGa₃O₁₂:Ce³⁺ Phosphor for near-UV Pumped White-LEDs. *RSC Adv.* **2016**, *6*, 2155–2161.
- (39) Zhong, J.; Zhao, W.; Du, F.; Wen, J.; Zhuang, W.; Liu, R.; Duan, C. K.; Wang, L.; Lin, K. Identifying the Emission Centers and Probing the Mechanism for Highly Efficient and Thermally Stable Luminescence in the La₃Si₆N₁₁:Ce³⁺ Phosphor. *J. Phys. Chem. C* **2018**, *122*, 7849–7858.
- (40) DOE BTO SSL Program, “2018 Solid-State Lighting R&D Opportunities,” edited by James Brodrick, Ph.D.
- (41) Urbach, F. Zur Lumineszenz Der Alkalihalogenide. *Sitzungsber. Akad. Wiss. Wien* **1930**, *139*, 363–372.
- (42) Denault, K. A.; Brgoch, J.; Kloß, S. D.; Gaultois, M. W.; Siewenie, J.; Page, K.; Seshadri, R. Average and Local Structure, Debye Temperature, and Structural Rigidity in Some Oxide Compounds Related to Phosphor Hosts. *ACS Appl. Mater. Interfaces* **2015**, *7*, 7264–7272.
- (43) Tian, Y. Development of Phosphors with High Thermal Stability and Efficiency for Phosphor-Converted LEDs. *J. Solid State Light.* **2014**, *1*, No. 11.